
HOW FAITHFUL IS TRAJECTORY-BASED DATA ATTRIBUTION? ERROR SOURCES, REMEDIES, AND PRACTICAL GUIDELINES

A PREPRINT

Junwei Deng^{1*}, Pingbang Hu¹, Suliang Jin², Hao Lu³, Jiachen T. Wang³, Shichang Zhang⁴, Jiaqi W. Ma¹

¹University of Illinois Urbana-Champaign

²University of Michigan

³Princeton University

⁴Harvard University

May 20, 2026

ABSTRACT

Trajectory-based data attribution methods estimate the influence of training samples on model predictions by unrolling the training trajectory. They are widely used in applications such as data selection, data valuation, and model diagnosis, but there is a lack of comprehensive error analysis of these methods, raising concerns about method faithfulness and hindering reliable deployment. In this work, we provide the first systematic analysis of error sources in trajectory-based data attribution, together with concrete remedies to mitigate them and practical guidelines for downstream use. We organize the total error into three categories, *config-level*, *algorithm-level*, and *system-level*. Building on this taxonomy, we make three contributions. First, we identify optimizer mismatch as the dominant config-level error: existing methods derive their attribution under the assumption of SGD, even for models trained with the modern de facto optimizer AdamW. We propose AdamW-influence to fully account for AdamW’s optimization dynamics, yielding improvements from 10% to over 300% in Spearman correlation between estimated and ground-truth influence across four settings spanning MLP, CNN, GPT-2, and Llama 3.2-1B. Second, we isolate the remaining algorithm-level error arising from the first-order Taylor approximation, identify the learning rate and trajectory length as factors governing the error magnitude, and derive a closed-form error proxy that can be evaluated along the original trajectory without retraining. Third, we translate these insights into practical guidelines for data selection by unifying offline and online strategies under a K -step look-ahead framework. Under this framework, online selection with a short horizon often matches or exceeds offline, and the optimal horizon can be tuned jointly with the learning rate. Together, these results turn the framework into an actionable selection recipe for practitioners.

1 Introduction

As modern AI systems increasingly rely on large-scale training data, *data attribution*, which estimates the influence of individual training samples on model behavior, has emerged as a central tool for improving performance and explainability (Deng et al., 2025). Among existing approaches, *trajectory-based data attribution* (hereafter, *trajectory-based attribution*), such as SGD-influence (Hara et al., 2019), TracIn (Pruthi et al., 2020), SOURCE (Bae et al., 2024), and DVEmb (Wang et al., 2025b), has emerged as the research frontier of data attribution. These methods relax the strong convexity and convergence assumptions that influence-function-style methods rely on but that rarely hold in modern deep learning (Bae et al., 2022). Trajectory-based attribution underlies a growing range of applications, e.g., data cleaning (Hara et al., 2019), data selection (Wang et al., 2024; Xia et al., 2024; Hu et al., 2026), data valuation (Wang et al., 2025a), and model diagnosis (Zhang et al., 2025; Wang et al., 2025b). Recent advances, such

*Email: junweid2@illinois.edu

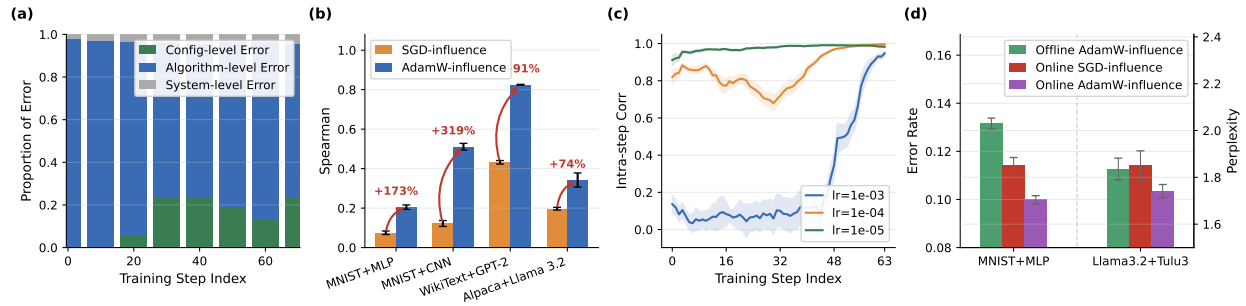


Figure 1: **An error taxonomy of trajectory-based attribution and our three key contributions.** (a) **Three error sources and how their proportion changes along the training trajectory.** The absolute error of SGD-influence on MNIST+MLP decomposes into config-level (green, optimizer mismatch), algorithm-level (blue, first-order Taylor), and system-level (gray) components. (b) **The proposed AdamW-influence algorithm corrects the dominant config-level error.** AdamW-influence (blue) improves over SGD-influence (orange) significantly in attribution fidelity measured by the Spearman ρ against TSLOO ground truth across four settings. (c) **Dissecting the algorithm-level error shows that learning rate and trajectory length are governing factors.** Intra-step Spearman ρ of AdamW-influence rises as the learning rate decreases and as training steps approach the trajectory end (shorter remaining trajectory). (d) **Our error corrections through aligned optimizer and short-horizon attribution can significantly boost data selection quality.** Online AdamW-influence (purple) outperforms online SGD-influence (red) and offline AdamW-influence (green) on MLP image classification (error rate, \downarrow) and Llama 3.2-1B SFT on Tulu3 (perplexity, \downarrow).

as gradient decomposition and random projection (Wang et al., 2025a), have further scaled these methods to modern model sizes, bringing them from a conceptual tool to a practical one.

As trajectory-based attribution matures into a practical tool driving downstream decisions, the reliability of these decisions hinges directly on the accuracy of the attribution scores. Yet practitioners deploying these attribution methods today cannot answer fundamental questions that arise in practice: How large is the attribution error in a training run? Where does the error originate, from a mismatch between the attribution formula and the actual training dynamics, or from approximations inherent in the algorithm itself? And how do routine training choices, such as the optimizer or the learning rate, affect the error? Despite the growing deployment of trajectory-based attribution, no systematic analysis answers these questions, leaving downstream applications exposed to attribution errors of unknown magnitude and origin, hindering broader deployment of these methods in practice.

In this work, we provide **the first systematic error analysis of trajectory-based attribution, with remedies and practical guidelines for its downstream deployment.** We specifically focus on the state-of-the-art efficient version (Wang et al., 2025b) of SGD-influence (Hara et al., 2019) method for our analysis. We organize the total attribution error into three categories (Figure 1a). *Config-level error* arises when the attribution formula does not faithfully reflect the actual training procedure, e.g., optimizer, batch composition, data curriculum or learning rate schedule. *Algorithm-level error* arises from approximations for efficiency, such as the first-order Taylor expansion. *System-level error* that is generally irreducible by algorithm design, such as errors caused by floating-point precision and GPU non-determinism. Building on this taxonomy, we make three contributions: analysis and a new algorithm to address the config-level error, dissection and proxy to remedy the algorithm-level error, and translating these analyses into practical guidelines for an impactful downstream application: data selection.

To address config-level error, we focus on its most impactful source: *optimizer mismatch*. Existing methods (Hara et al., 2019; Wang et al., 2025b; Pruthi et al., 2020) derive their attribution under the assumption of SGD, yet modern models (Grattafiori et al., 2024; Dosovitskiy et al., 2020) are almost universally trained with AdamW (Loshchilov and Hutter, 2017), introducing systematic deviation at every attribution step. We propose **AdamW-influence**, which correctly accounts for AdamW’s momentum states and coordinate-wise scaling. Across four settings spanning MLP, CNN, GPT-2, and Llama 3.2-1B, it improves the Spearman correlation between estimated and ground-truth influence by 10% to over 300% against the SGD-based baseline (Figure 1b). This correction is also the necessary first step before the remaining algorithm-level error can be cleanly isolated.

With config-level error corrected, we turn to the algorithm-level error from the *first-order Taylor expansion*. We identify **two factors that govern its magnitude, the learning rate and the trajectory length**, controlling per-step magnitude and accumulation depth, respectively (Figure 1c). At the per-sample level, we further derive a closed-form error proxy evaluable along the original trajectory without retraining, which correlates strongly (Spearman $\rho \in [0.83, 0.89]$) with ground-truth error norms from trajectory-specific leave-one-out retraining.

Finally, we translate these insights into **practical guidelines for data selection**, unifying offline and online strategies under a K -step look-ahead framework, where K controls the horizon over which attribution informs selection. Our error analysis directly explains three empirical findings (Figure 1d): optimizer alignment transfers from attribution fidelity to selection performance, with online AdamW-influence outperforming its SGD-based baseline; online selection with small to moderate K matches or exceeds offline, since offline corresponds to the longest horizon and accumulates the largest error; and the optimal K grows as the learning rate decreases, since smaller per-step learning rates allow the K -step summation to extend further before error dominates. These results turn the error analysis to actionable selection recipe for practitioners.

2 Error analysis of trajectory-based data attribution

2.1 Preliminaries: trajectory-based attribution and SGD-influence

Trajectory-based data attribution methods evaluate a data point’s influence by tracing the exact sequence of mini-batches and the dynamics of the training process, rather than relying only on the final model parameters. Consider an optimization process that runs for T steps, yielding a parameter trajectory $\theta_0, \theta_1, \dots, \theta_T$. Let z^* be a training data point in mini-batch \mathcal{B}_{t^*} at iteration t^* . The exact counterfactual impact of removing z^* from the parameter update at step t^* on the loss at a validation point $z^{(\text{val})}$ is the Trajectory-Specific Leave-One-Out (TSLOO) error, originally conceptualized by Hara et al. (2019):

$$\text{TSLOO}(z^*; z^{(\text{val})}) := \ell(\theta'_{T, z^*}, z^{(\text{val})}) - \ell(\theta_T, z^{(\text{val})}), \quad (1)$$

where $\theta'_{T, z^*} \in \mathbb{R}^p$ is the final model parameters obtained if z^* had been excluded from the parameter update at step t^* , and p is the parameter size.

Hara et al. (2019) approximate the TSLOO error via a first-order Taylor expansion of the parameter trajectory in a perturbation scalar ϵ injected at step t^* , yielding the *SGD-influence*:

$$\ell(\theta'_{T, z^*}, z^{(\text{val})}) - \ell(\theta_T, z^{(\text{val})}) \approx \eta_{t^*} \nabla_{\theta} \ell(\theta_T, z^{(\text{val})})^{\top} \left[\prod_{t=t^*+1}^{T-1} (I - \eta_t H_t) \right] \nabla_{\theta} \ell(\theta_{t^*}, z^*), \quad (2)$$

where η_t is the learning rate and $H_t = \nabla_{\theta}^2 \ell(\theta_t, \mathcal{B}_t)$ is the per-step Hessian. Wang et al. (2025b) reduce the cost to $\mathcal{O}(T)$ under the GGN approximation $H_t \approx \frac{1}{|\mathcal{B}_t|} \sum_{z \in \mathcal{B}_t} g_{t,z} g_{t,z}^{\top}$ (with $g_{t,z} = \nabla_{\theta} \ell(\theta_t, z)$) by extracting test-independent components into per-sample embeddings, computed via a backward recurrence over a summary matrix $W^{(t)} \in \mathbb{R}^{p \times p}$. We refer to this efficient implementation as SGD-influence throughout this paper and defer a detailed discussion of Wang et al. (2025b)’s implementation to Appendix A.

2.2 The error sources of trajectory-based attribution

The *attribution error* is the discrepancy between the estimated attribution score and the ground-truth TSLOO (Eq. 1). We organize its sources along the trajectory into three categories: config-level, algorithm-level, and system-level.

Config-level error. Config-level error arises whenever the attribution formula does not faithfully reflect a component of the actual training procedure. Potential sources include the optimizer, batch composition, data curriculum, and learning rate schedule. Among these, batch composition, data curriculum and learning rate schedule are aligned straightforwardly by replaying the recorded training log, and SGD-influence already incorporates both. *Optimizer mismatch*, by contrast, is neither addressed by existing methods nor trivial to correct: current methods derive their attribution under the assumption of SGD (Hara et al., 2019; Wang et al., 2025b), even for models trained with modern de facto optimizer AdamW. In Section 3, we address this dominant config-level error and show that the correction will significantly improve attribution fidelity.

Algorithm-level error. Even when the attribution formula perfectly matches the training dynamics, computing the exact TSLOO is intractable for nonlinear models, and trajectory-based attribution relies on approximations such as a first-order Taylor expansion of the parameter trajectory. Algorithm-level error is the gap introduced by these approximations, and its profile depends on the specific approximation strategy. We analyze it in the context of AdamW-influence, whose attribution relies on a first-order Taylor expansion. In Section 4, we dissect this error, identify the factors governing its magnitude, and derive a closed-form proxy for per-sample analysis.

System-level error. System-level errors, such as floating-point precision and GPU non-determinism, are not specific to attribution methods, and even compute the TSLOO by directly retraining the model also suffer from this type of error. Therefore, they are largely irreducible by attribution algorithm design. Empirically, we find this irreducible part to be relatively small compared to the total error. We thus focus on analyzing and reducing the other two types of errors.

3 Correcting the dominant config-level error: AdamW-influence

As established in Section 2.2, optimizer mismatch is the dominant source of config-level error and requires non-trivial solution. In Section 3.1, we derive AdamW-influence, which extends the SGD-influence to correctly account for the modern de facto optimizer AdamW (Loshchilov and Hutter, 2017). We then evaluate its attribution fidelity in Section 3.2, demonstrating substantial improvements across four settings.

3.1 AdamW-influence

Both SGD-influence and AdamW-influence estimate the same TSLOO target (Eq. 1) but unroll different optimizers along the trajectory. SGD-influence unrolls the SGD updates for simplicity, even when the trajectory is actually from a different optimizer such as AdamW. Our AdamW-influence performs the analogous estimate but unrolls the actual AdamW updates.

Challenges for unrolling the AdamW updates. Two features distinguish AdamW from SGD and make the AdamW unrolling non-trivial: (i) momentum and second-moment states that carry perturbations across steps, and (ii) a coordinate-wise adaptive scaling that makes the update nonlinear in the gradient. The SGD-influence derivation hinges on the update being linear in the per-step gradient, so that injecting a parameter-level perturbation is equivalent to removing z^* from the batch. Under AdamW this equivalence breaks: the second moment depends quadratically on the gradient and enters the update nonlinearly through the denominator, so a parameter-level perturbation no longer corresponds to removing z^* from the batch.

AdamW unrolling. To address this, AdamW-influence injects the perturbation at the gradient level rather than the parameter level, and propagates it through the joint dynamics of the parameters and the two moment states.

Proposition 1 (AdamW-influence, informal). *The AdamW-influence score for every training sample can be computed in $\mathcal{O}(T)$ via a backward recurrence over the training trajectory, matching the asymptotic complexity of SGD-influence.*

The proof extends the backward computation of SGD-influence, with the main challenge and innovation being the propagation of the gradient-level perturbation through AdamW’s coupled moment states and adaptive scaling. The full derivation, transition operators, and per-sample recurrence are deferred to Appendix B, and the cost analysis to Appendix C.

3.2 Fidelity evaluation

We evaluate the attribution fidelity of AdamW-influence against the SGD-influence baseline by measuring the Spearman rank correlation between predicted attribution scores and ground-truth TSLOO scores (Eq. 1) obtained via retraining. Results in Table 1 show that AdamW-influence outperforms SGD-influence in four settings: an MLP and a CNN trained on MNIST, GPT-2 continually pretrained on WikiText-2, and Llama 3.2-1B fine-tuned on Alpaca. The improvements range from 10% to over 300%. For each setting, we also vary the learning rate, which we find to be an important factor in the error and study systematically in Section 4. Full training details and hyperparameters are provided in Appendix D.

4 Dissecting the algorithm-level error

Section 3 corrected the dominant config-level error by aligning the attribution formula with the AdamW dynamics. We now turn to the algorithm-level error, which arises from the first-order Taylor expansion that AdamW-influence² uses to make attribution tractable. This section dissects the algorithm-level error in three steps. Section 4.1 empirically locates its dominant error source, isolating the *update-estimation error* as the bottleneck. Section 4.2 identifies the two factors, learning rate and trajectory length, that jointly govern its magnitude. Section 4.3 derives a closed-form error proxy that estimates per-sample error along the original training trajectory without retraining.

4.1 Dominant error from estimating the parameter update

Recall from Section 2.2 that the algorithm-level error of AdamW-influence decomposes into the *update-estimation error*, the gap between the true parameter update $\Delta\theta_{z^*} = \theta'_{T,z^*} - \theta_T$ and estimated parameter update AdamW-influence $_{z^*}$, and a *residual* collecting higher-order terms and system-level error. To locate which component dominates, and to quantify how much of the total attribution error was previously absorbed by optimizer mismatch, we decompose the

²And other trajectory-based attribution methods (Hara et al., 2019; Wang et al., 2025b) more broadly.

Table 1: Fidelity comparison (Spearman ρ against TSLOO ground truth) between AdamW-influence and SGD-influence when training with **AdamW**. Best result per row in **bold**. $\Delta\%$ is the relative improvement of AdamW-influence over SGD-influence. Full results across all data sizes in Appendix E.1.

Setting	LR	AdamW-influence	SGD-influence	$\Delta\%$
MNIST+MLP	1e-3	0.205±0.011	0.075±0.009	+173%
	1e-4	0.294±0.014	0.242±0.016	+21%
	1e-5	0.786±0.013	0.715±0.012	+10%
MNIST+CNN	1e-3	0.090±0.008	0.015±0.009	+500%
	1e-4	0.511±0.017	0.122±0.015	+319%
	1e-5	0.791±0.007	0.526±0.007	+50%
WikiText+GPT-2	1e-4	0.734±0.003	0.372±0.006	+97%
	5e-5	0.825±0.002	0.432±0.009	+91%
	1e-5	0.842±0.006	0.480±0.015	+75%
Alpaca+Llama 3.2	6e-6	0.276±0.047	0.156±0.019	+77%
	2e-6	0.342±0.036	0.197±0.007	+74%
	5e-7	0.665±0.013	0.330±0.017	+102%

absolute SGD-influence error of a sample z^* into three additive components:

$$|\text{Error}_{\text{SGD}_{z^*}}| = \underbrace{|\text{Error}_{\text{SGD}_{z^*}}| - |\text{Error}_{\text{AdamW}_{z^*}}|}_{\text{Green: optimizer mismatch}} + \underbrace{|\nabla\ell(\theta_T, z^{(\text{val})}) \cdot (\Delta\theta_{z^*}^* - \text{AdamW-influence}_{z^*})|}_{\text{Blue: update-estimation error}} + \underbrace{\text{rest}}_{\text{Grey: residual}}, \quad (3)$$

$|\text{Error}_{\text{SGD}_{z^*}}|$ and $|\text{Error}_{\text{AdamW}_{z^*}}|$ are the absolute errors of influence estimate by SGD-influence and AdamW-influence with the TSLOO ground-truth, respectively. The green term measures the error share corrected by AdamW-influence; the blue term is the update-estimation error remaining after optimizer alignment; the grey term collects all higher-order remainders and system-level error.

Figure 2 reports this decomposition on an MLP trained on MNIST across three learning rates (10^{-3} , 10^{-4} , 10^{-5}), with errors aggregated into bins of 5 training steps (full setup in Appendix D). Two patterns stand out. (1) Once optimizer mismatch is corrected, **the update-estimation error accounts for the overwhelming majority** of the remaining error, while the higher-order residual is consistently small. We thus focus on analyzing and correcting the dominant update-estimation error for the rest of this section. (2) The optimizer-mismatch share grows as the learning rate decreases and as training progresses, indicating that **optimizer alignment becomes more important in low learning rate or short trajectory length cases**—precisely the regimes most relevant to data selection in our later analysis.

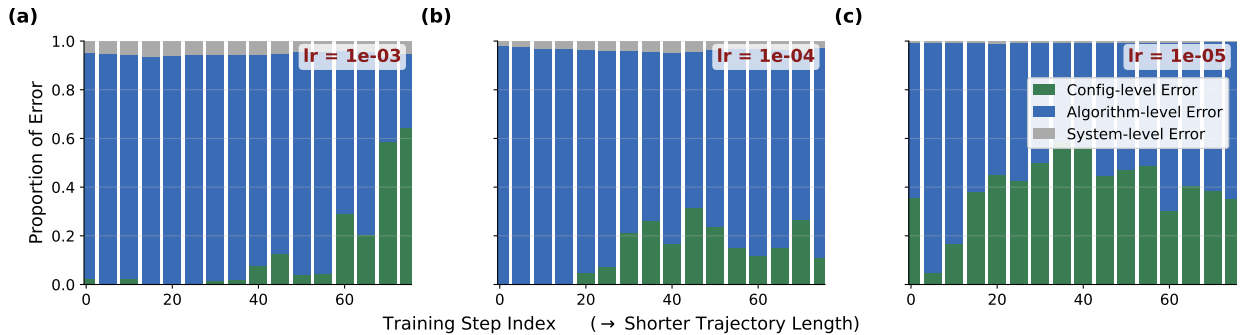


Figure 2: **Decomposition of $|\text{Error}_{\text{SGD}}|$ across the training trajectory of an MLP trained on MNIST.** Panels (a)–(c) sweep three learning rates: (a) $\eta = 10^{-3}$, (b) $\eta = 10^{-4}$, (c) $\eta = 10^{-5}$. The absolute SGD-influence error is decomposed into three additive components, where each category is represented by its dominant source: **Green**, config-level error from optimizer mismatch, the share fixed by switching to AdamW-influence; **Blue**, algorithm-level error from the first-order Taylor expansion (the update-estimation error remaining after optimizer alignment); and **Grey**, residual error absorbing all higher-order remainders together with system-level effects (e.g., floating-point precision, GPU non-determinism). Errors are aggregated into bins of 5 training steps; larger step indices correspond to shorter remaining trajectory length $T - t^*$.

4.2 Two factors governing the algorithm-level error

Having established that the update-estimation error dominates the algorithm-level error, we investigate what governs its magnitude. The error has an intuitively simple structure: at each step, a first-order Taylor expansion linearizes the parameter update around the unperturbed trajectory, incurring a per-step error whose magnitude scales with the size of that step; these per-step errors then accumulate as the perturbation propagates to the end of training. This structure points to two controllable training quantities: the *learning rate*, which sets the magnitude of each per-step parameter update and thus the per-step linearization error; and the *trajectory length* $T - t^*$, the distance from the injection step t^* to the trajectory terminal T , which determines how many per-step errors are summed into the final attribution error.

To verify the influence of each factor, we sweep three learning rates on an MLP and a CNN trained on MNIST, evaluating attribution quality across the trajectory through two metrics: the *error norm* $\|\Delta\theta_{z^*} - \text{AdamW-influence}_{z^*}\|^2$, which directly measures parameter-space error (lower is better); and the *intra-step Spearman correlation* between attributed and ground-truth per-sample influences within each training step, which reflects the ability to rank samples within a batch (higher is better). Since the trajectory length $T - t^*$ is itself indexed by the training step, a single sweep over training steps traces both factors at once, with each curve isolating the learning-rate effect at a fixed trajectory length.

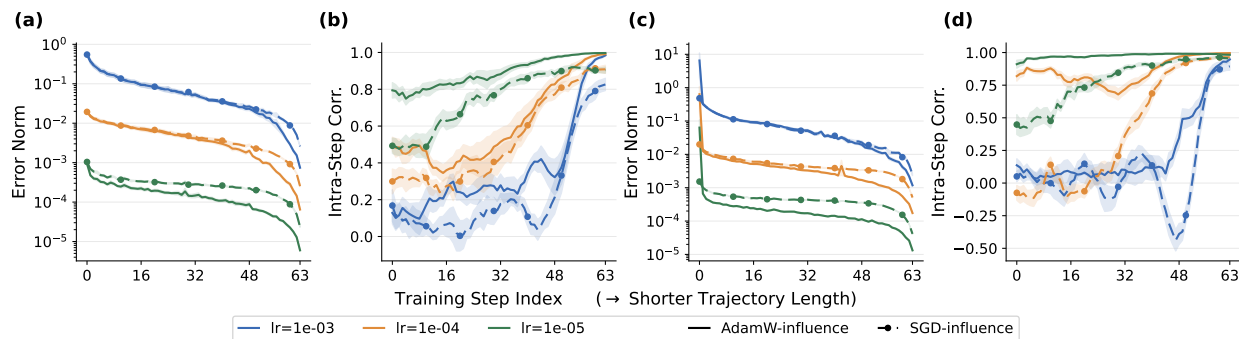


Figure 3: **Error norm and intra-step Spearman correlation across three learning rates**, on (a, b) an MLP and (c, d) a CNN trained on MNIST. Panels (a, c) report error norm (\downarrow); panels (b, d) report intra-step Spearman correlation (\uparrow , smoothed over 5 consecutive steps). The training step index runs from 0 to $T - 1$; larger indices correspond to *shorter* trajectory lengths $|T - t^*|$, since the perturbation has fewer remaining steps to propagate. AdamW-influence (solid) and SGD-influence (dashed) are shown for reference.

Learning rate. Larger learning rates push per-step parameter updates further from the linearization point, amplifying the higher-order terms that the first-order approximation discards. Figure 3 confirms this dependence across architectures and metrics: the error norm increases monotonically with the learning rate throughout the trajectory, and the intra-step correlation degrades correspondingly, with $\eta = 10^{-5}$ ($\eta = 10^{-3}$) achieving the highest (lowest) correlation throughout training.

Trajectory length. Independently of the magnitude of each step, errors propagate and accumulate along the training trajectory. In Figure 3, we see that as the trajectory length $T - t^*$ shrinks (i.e., as the training step index approaches T), the error norm decreases and the intra-step correlation increases across all three learning rates. **Notably, AdamW-influence reaches near-perfect intra-step correlation at very short trajectory lengths for all three learning rates**, indicating that short-horizon attribution is reliable even at learning rates where full-trajectory attribution is noisy. This compounding behavior between the two factors will be central to the practical implications in Section 5.

4.3 Error proxy

Beyond identifying trajectory-level factors that govern attribution error magnitude, we also try to identify per-sample errors to facilitate applications like data selection. Computing per-sample error directly requires TSLOO retraining that is computationally prohibitive. We thus derive a closed-form *error proxy* that can be evaluated along the original training trajectory.

Proposition 2 (Error proxy for update-estimation error). *Under the AdamW training dynamics in Section 3.1, the update-estimation error at the final step admits a closed-form expression as the sum of per-step residuals $r_t \in \mathbb{R}^p$*

propagated through the linearized dynamics, where per-coordinate residual $r_{t,i}$ is

$$|r_{t,i}| \sim \eta_t \left(\frac{\|\dot{\theta}_t\|^2}{\sqrt{\hat{v}_{t,i}}} + \frac{[H_t \dot{\theta}_t]_i^2}{\hat{v}_{t,i}} \right). \quad (4)$$

Here $\dot{\theta}_t$ denotes the parameter perturbation propagated by AdamW-influence (the derivative of the parameter trajectory with respect to the injected perturbation ϵ at $\epsilon = 0$), and $\hat{v}_{t,i}$ is AdamW’s bias-corrected second-moment estimate at coordinate i . The full unrolled form and derivation are deferred to Appendix F.

Equation (4) reflects the two error governing factors in Section 4.2. Per-step scaling by η_t and accumulation over trajectory length, and additionally exposes a sample-distinguishing term $\|\dot{\theta}_t\|^2 + [H_t \dot{\theta}_t]_i^2$ that captures training-stage effects unique to each sample.

We validate the proxy against ground-truth error norms on an MLP and a CNN trained on MNIST, each at two learning rates. Figure 4 shows Spearman rank correlation $\rho \in [0.83, 0.89]$ across all four settings. Crucially, the proxy reuses quantities already maintained by AdamW-influence plus one Hessian-vector product per step, keeping total cost at $\mathcal{O}(T)$. It makes the proxy a practical signal for trajectory-aware decisions downstream, including the error-driven horizon analysis in Section 5.

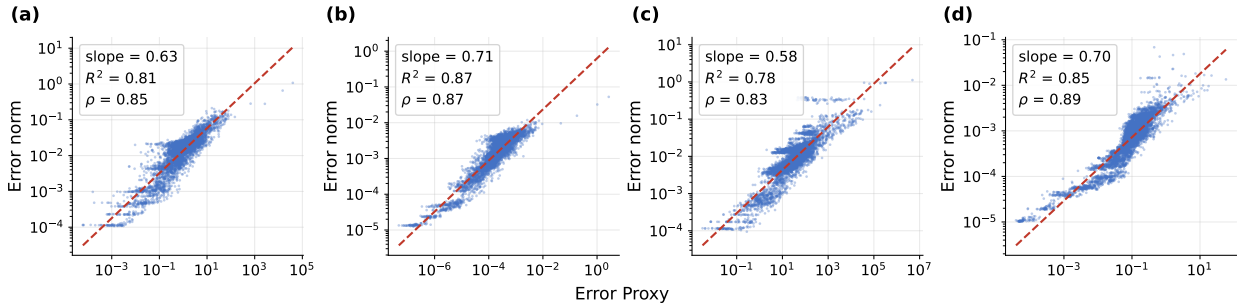


Figure 4: **The error proxy tracks the ground-truth error norm $\|\Delta\theta - \text{AdamW-influence}\|$ across training samples.** Each point is a single training sample; axes are on log-log scale. Panels: (a) MLP, $\eta = 10^{-3}$; (b) MLP, $\eta = 10^{-4}$; (c) CNN, $\eta = 10^{-3}$; (d) CNN, $\eta = 10^{-4}$. Both architectures are trained on MNIST. The red dashed line is a linear fit; insets report its slope and R^2 , along with the Spearman rank correlation ρ between proxy and ground truth.

5 Practical implications in data selection

Sections 3 and 4 together provide a systematic understanding of where the error in trajectory-based attribution originates and how to mitigate it. We now translate these insights into practical guidelines for data selection, one of the most consequential downstream applications of trajectory-based attribution. Specifically, we use the error analysis to predict which selection strategies should work better and verify these predictions empirically.

5.1 A unified K -Step look-ahead framework for data selection

Trajectory-based attribution can be used for data selection in two ways: *offline*, which runs a full training pass, computes attribution against a held-out validation set using the entire trajectory, and retrains from scratch on the selected subset; and *online*, which selects samples on-the-fly during a single training run using a short-horizon attribution score evaluated at the current parameters Deng et al. (2025). Despite their procedural differences, we show that they can be conceptually unified along a single axis: the look-ahead horizon of each selection decision.

Unified K -Step Setup. The horizon K controls how far ahead each candidate is scored. At step t , instead of asking “does including z help validation loss right now?” we ask “does including z help validation loss K steps from now?”. Larger K looks further into the future and captures more downstream effect; smaller K stays close to the present.

Concretely, at each step t we draw a random candidate batch \mathcal{C}_t of size N , score each candidate $z \in \mathcal{C}_t$ by $s_t^{(K)}(z) = \nabla_{\theta} \ell(\theta_t, z^{(\text{val})})^\top \dot{\theta}_{t+K+1}(z)$, and retain the top- B as \mathcal{B}_t for the parameter update. Here $\dot{\theta}_{t+K+1}(z)$ is the parameter perturbation K steps after injecting z at step t , computed via the AdamW-influence recurrence of Section 3. Algorithm 2 (Appendix G) gives the pseudo-code.

This single knob recovers existing strategies as boundary cases: $K = 0$ is the per-step scoring rule used by GREATS Wang et al. (2024) (without its greedy selection iteration), and $K = T - t$ is full-trajectory propaga-

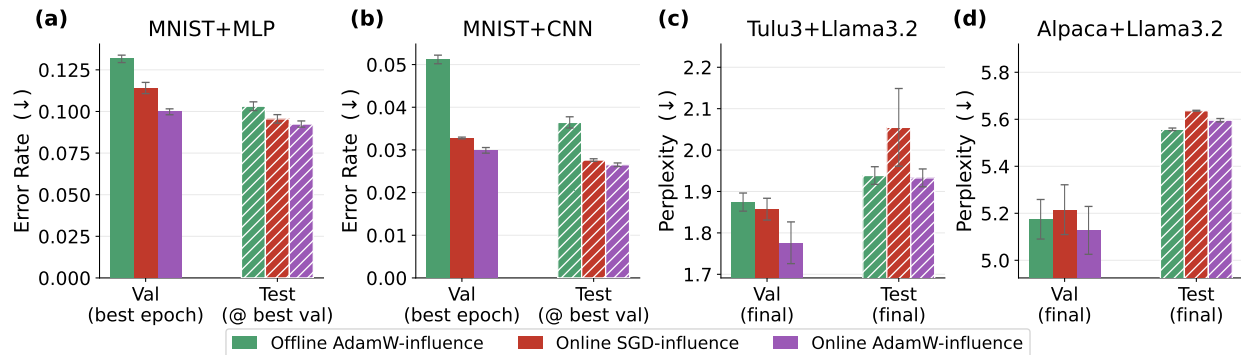


Figure 5: **Online AdamW-influence consistently outperforms online SGD-influence, and matches or exceeds offline AdamW-influence across four settings.** (a) an MLP and (b) a CNN trained on MNIST (error rate, \downarrow); Also, Llama 3.2-1B fine-tuned on (c) Tulu3 and (d) Alpaca (perplexity, \downarrow). For MNIST settings, “Val” is at the best epoch and “Test” is reported at that epoch; for Llama 3.2-1B settings, both are at the final step. $K = 10$ for MLP, $K = 5$ for CNN, and $K = 2$ for Llama 3.2-1B.

tion, intractable to run online but approximated by offline selection on a completed reference trajectory. Online selection with finite K thus scans the intermediate horizons between these two extremes. This exposes K directly to the error analysis of Section 4: larger K accumulates more approximation error, while smaller K discards information about downstream dynamics.

5.2 Practical implications and error-analysis explanations

We experiment on four settings with optimizer AdamW, comparing “offline AdamW-influence”, “online SGD-influence”, and “online AdamW-influence” with varying K . Full setup in Appendix D.3.

Optimizer alignment transfers to downstream selection. Online AdamW-influence outperforms online SGD-influence in all settings (Figure 5), mirroring the attribution-fidelity gains of Section 3.2. The dominant config-level error identified in Section 2.2 thus propagates directly into selection quality: a selection rule built on a mis-specified optimizer undermines selection performance.

Horizon K trades off lookahead information against attribution error. Larger K collects more information about a candidate’s future effect but accumulates more first-order approximation error per Section 4.2; smaller K keeps error low but reflects only short-range effects. We observe this trade-off between online and offline results: in all four settings, online AdamW-influence with a small-to-moderate K matches or exceeds offline AdamW-influence (Figure 5), consistent with offline corresponding to the longest horizon $K = T - t - 1$ and accumulating the largest error. We do not claim offline is universally inferior. When we have small learning rate, short training, or late-stage fine-tuning, offline can remain competitive or superior. Within the practical training regimes considered here, online with a small-to-moderate K is a reliable choice.

The optimal K shifts with the learning rate. Sweeping $K \in \{2, 5, 10, 25\}$ across three learning rates on MNIST (Figure 6), the best K is 5 at $\eta = 10^{-2}$, 10 at $\eta = 10^{-3}$, and 25 at $\eta = 10^{-4}$: the optimal horizon grows as the learning rate shrinks. This is precisely what Section 4.2 predicts: larger K collects more information about how a candidate influences future training but accumulates more approximation error, and the optimal K balances these two effects. A practical guidance is that K should be tuned jointly with the learning rate rather than fixed across runs; a larger K is not necessarily better.

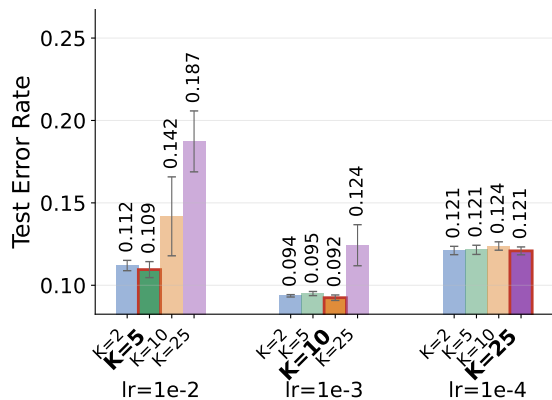


Figure 6: The optimal K increases as the learning rate decreases. We sweep $K \in \{2, 5, 10, 25\}$ across three learning rates using online AdamW-influence for MLP on MNIST. Bars show test error rate at the best validation epoch; the best K per learning rate is highlighted in red.

6 Related work

Trajectory-based data attribution. Convergence-based methods, influence functions (Koh and Liang, 2017; Grosse et al., 2023), TRAK (Park et al., 2023), and LoGra (Choe et al., 2026), rely on convergence or permutation-invariance assumptions violated by modern stochastic training (Wang et al., 2025b). Trajectory-based attribution methods mitigate these by attributing along the optimization path: SGD-influence (Hara et al., 2019), TracIn (Pruthi et al., 2020), SOURCE (Bae et al., 2024), and DVEmb (Wang et al., 2025b). Recent extensions handle cross-epoch compounding under SGD (Shi et al., 2025) or stage-level effects with momentum and weight decay (Zhang et al., 2025), but none cover AdamW’s second-moment coupling at the per-sample level, and all are proposed as standalone methods without comprehensive error analysis. We extend trajectory-based attribution to AdamW and provide the first error taxonomy with a careful analysis.

Data attribution for data selection. *Offline selection* retrains on a subset chosen using attribution from a completed reference trajectory; representative work includes LESS (Xia et al., 2024), which adapts *single-step* influence to Adam. *Online selection* chooses samples on-the-fly: GREATS (Wang et al., 2024) uses a Taylor approximation of the immediate validation effect. Beyond unrolling-based attribution, MATES (Yu et al., 2024) fits a small data-influence model to oracle scores collected by locally probing the pretraining model, sidestepping first-order approximation entirely at the cost of training an auxiliary model. We unify both regimes into a unified framework.

7 Conclusion

We presented the first systematic error analysis of trajectory-based data attribution. By organizing the error into a three-level taxonomy, we develop AdamW-influence to remedy the dominant config-level error, identify the learning rate and trajectory length as the two factors governing the algorithm-level error, and derive a closed-form proxy for per-sample algorithm-level error. Building on this analysis, we further provide actionable guidelines for data selection through a unified K -step look-ahead framework. We see this as a step toward treating attribution methods as diagnosable estimators rather than black-box scoring functions. The taxonomy and the error analysis provide a foundation for trajectory-based attribution to scale to larger models and be deployed for broader applications.

Limitations. Our analysis is restricted to trajectory-based attribution methods that use first-order Taylor since these methods represent the state-of-the-art, but extending the error taxonomy to other attribution methods remains open, such as MAGIC (Ilyas and Engstrom, 2025) and Simfluence (Guu et al., 2023). Our LLM experiments are limited to models up to Llama 3.2-1B due to computation constraints, and validation at larger scales is left to future work. Our empirical evaluation focuses on supervised classification and language modeling; whether the same error patterns and practical guidelines transfer to other regimes such as reinforcement learning or diffusion models is an important direction for future investigation.

References

- Juhan Bae, Nathan Ng, Alston Lo, Marzyeh Ghassemi, and Roger B Grosse. If influence functions are the answer, then what is the question? *Advances in Neural Information Processing Systems*, 35:17953–17967, 2022.
- Juhan Bae, Wu Lin, Jonathan Lorraine, and Roger Grosse. Training data attribution via approximate unrolling. *Advances in Neural Information Processing Systems*, 37:66647–66686, 2024.
- Sang Keun Choe, Hwijee Ahn, Juhan Bae, Kewen Zhao, Youngseog Chung, Adithya Pratapa, Willie Neiswanger, Emma Strubell, Teruko Mitamura, Jeff Schneider, Eduard Hovy, Roger Baker Grosse, and Eric P. Xing. What is your data worth to GPT? LLM-scale data valuation with influence functions. In *The Thirty-ninth Annual Conference on Neural Information Processing Systems*, 2026. URL <https://openreview.net/forum?id=zPKeJAEo27>.
- Jonathan H Clark, Eunsol Choi, Michael Collins, Dan Garrette, Tom Kwiatkowski, Vitaly Nikolaev, and Jennimaria Palomaki. Tydi qa: A benchmark for information-seeking question answering in ty pologically di verse languages. *Transactions of the Association for Computational Linguistics*, 8:454–470, 2020.
- Junwei Deng, Yuzheng Hu, Pingbang Hu, Ting-Wei Li, Shixuan Liu, Jiachen T Wang, Dan Ley, Qirun Dai, Benhao Huang, Jin Huang, et al. A survey of data attribution: Methods, applications, and evaluation in the era of generative ai. 2025.
- Alexey Dosovitskiy, Lucas Beyer, Alexander Kolesnikov, Dirk Weissenborn, Xiaohua Zhai, Thomas Unterthiner, Mostafa Dehghani, Matthias Minderer, Georg Heigold, Sylvain Gelly, et al. An image is worth 16x16 words: Transformers for image recognition at scale. *arXiv preprint arXiv:2010.11929*, 2020.

- Bogdan Gliwa, Iwona Mochol, Maciej Biesek, and Aleksander Wawer. SAMSum corpus: A human-annotated dialogue dataset for abstractive summarization. In *Proceedings of the 2nd Workshop on New Frontiers in Summarization*, pages 70–79, Hong Kong, China, November 2019. Association for Computational Linguistics. doi: 10.18653/v1/D19-5409. URL <https://www.aclweb.org/anthology/D19-5409>.
- Aaron Grattafiori, Abhimanyu Dubey, Abhinav Jauhri, Abhinav Pandey, Abhishek Kadian, Ahmad Al-Dahle, Aiesha Letman, Akhil Mathur, Alan Schelten, Alex Vaughan, et al. The llama 3 herd of models. *arXiv preprint arXiv:2407.21783*, 2024.
- Roger Grosse, Juhan Bae, Cem Anil, Nelson Elhage, Alex Tamkin, Amirhossein Tajdini, Benoit Steiner, Dustin Li, Esin Durmus, Ethan Perez, et al. Studying large language model generalization with influence functions. *arXiv preprint arXiv:2308.03296*, 2023.
- Kelvin Guu, Albert Webson, Ellie Pavlick, Lucas Dixon, Ian Tenney, and Tolga Bolukbasi. Simfluence: Modeling the influence of individual training examples by simulating training runs. *arXiv preprint arXiv:2303.08114*, 2023.
- Satoshi Hara, Atsushi Nitanda, and Takanori Maehara. Data cleansing for models trained with sgd. *Advances in Neural Information Processing Systems*, 32, 2019.
- Yuzheng Hu, Fan Wu, Haotian Ye, David Forsyth, James Zou, Nan Jiang, Jiaqi W. Ma, and Han Zhao. A snapshot of influence: A local data attribution framework for online reinforcement learning. In *The Thirty-ninth Annual Conference on Neural Information Processing Systems*, 2026. URL <https://openreview.net/forum?id=sYK4yPDuT1>.
- Andrew Ilyas and Logan Engstrom. Magic: Near-optimal data attribution for deep learning. *arXiv preprint arXiv:2504.16430*, 2025.
- Pang Wei Koh and Percy Liang. Understanding black-box predictions via influence functions. In *International conference on machine learning*, pages 1885–1894. PMLR, 2017.
- Yann LeCun, Léon Bottou, Yoshua Bengio, and Patrick Haffner. Gradient-based learning applied to document recognition. *Proceedings of the IEEE*, 86(11):2278–2324, 2002.
- Ilya Loshchilov and Frank Hutter. Decoupled weight decay regularization. *arXiv preprint arXiv:1711.05101*, 2017.
- Stephen Merity, Caiming Xiong, James Bradbury, and Richard Socher. Pointer sentinel mixture models, 2016.
- Sung Min Park, Kristian Georgiev, Andrew Ilyas, Guillaume Leclerc, and Aleksander Madry. TRAK: Attributing model behavior at scale. In Andreas Krause, Emma Brunskill, Kyunghyun Cho, Barbara Engelhardt, Sivan Sabato, and Jonathan Scarlett, editors, *Proceedings of the 40th International Conference on Machine Learning*, volume 202 of *Proceedings of Machine Learning Research*, pages 27074–27113. PMLR, 23–29 Jul 2023. URL <https://proceedings.mlr.press/v202/park23c.html>.
- Garima Pruthi, Frederick Liu, Satyen Kale, and Mukund Sundararajan. Estimating training data influence by tracing gradient descent. *Advances in Neural Information Processing Systems*, 33:19920–19930, 2020.
- Alec Radford, Jeffrey Wu, Rewon Child, David Luan, Dario Amodei, Ilya Sutskever, et al. Language models are unsupervised multitask learners. *OpenAI blog*, 1(8):9, 2019.
- Yunxiao Shi, Shuo Yang, Yixin Su, Rui Zhang, and Min Xu. Accumulative sgd influence estimation for data attribution. *arXiv preprint arXiv:2510.26185*, 2025.
- Rohan Taori, Ishaan Gulrajani, Tianyi Zhang, Yann Dubois, Xuechen Li, Carlos Guestrin, Percy Liang, and Tatsunori B. Hashimoto. Stanford alpaca: An instruction-following llama model. https://github.com/tatsu-lab/stanford_alpaca, 2023.
- Jiachen T Wang, Tong Wu, Dawn Song, Prateek Mittal, and Ruoxi Jia. Greats: Online selection of high-quality data for llm training in every iteration. *Advances in Neural Information Processing Systems*, 37:131197–131223, 2024.
- Jiachen T. Wang, Prateek Mittal, Dawn Song, and Ruoxi Jia. Data shapley in one training run. In *The Thirteenth International Conference on Learning Representations*, 2025a. URL <https://openreview.net/forum?id=HD6bWcj87Y>.
- Jiachen T. Wang, Dawn Song, James Zou, Prateek Mittal, and Ruoxi Jia. Capturing the temporal dependence of training data influence. In *The Thirteenth International Conference on Learning Representations*, 2025b. URL <https://openreview.net/forum?id=uHLgDEgiS5>.
- Mengzhou Xia, Sadhika Malladi, Suchin Gururangan, Sanjeev Arora, and Danqi Chen. LESS: Selecting influential data for targeted instruction tuning. In Ruslan Salakhutdinov, Zico Kolter, Katherine Heller, Adrian Weller, Nuria Oliver, Jonathan Scarlett, and Felix Berkenkamp, editors, *Proceedings of the 41st International Conference on Machine Learning*, volume 235 of *Proceedings of Machine Learning Research*, pages 54104–54132. PMLR, 21–27 Jul 2024. URL <https://proceedings.mlr.press/v235/xia24c.html>.

Zichun Yu, Spandan Das, and Chenyan Xiong. MATES: Model-aware data selection for efficient pretraining with data influence models. In *The Thirty-eighth Annual Conference on Neural Information Processing Systems*, 2024. URL <https://openreview.net/forum?id=6gzPSMUaz2>.

Shichang Zhang, Hongzhe Du, Jiaqi W Ma, and Himabindu Lakkaraju. Who gets credit or blame? attributing accountability in modern ai systems. *arXiv preprint arXiv:2506.00175*, 2025.

A Detailed review of SGD-influence

For SGD-influence, Wang et al. (2025b) reduce the cost to $\mathcal{O}(T)$ under the GGN approximation $H_t \approx \frac{1}{|\mathcal{B}_t|} \sum_{z \in \mathcal{B}_t} g_{t,z} g_{t,z}^\top$ by extracting test-independent components into per-sample embeddings, computed via a backward recurrence over a summary matrix $W^{(t)} \in \mathbb{R}^{p \times p}$ that encodes how a perturbation injected at step t propagates through all subsequent training steps to the final parameters:

$$\text{SGD-influence}_z = \eta_t (I - W^{(t)}) g_{t,z}, \quad \forall z \in \mathcal{B}_t, \quad (5)$$

$$W^{(t-1)} = W^{(t)} + \frac{1}{|\mathcal{B}_t|} \sum_{z \in \mathcal{B}_t} \text{SGD-influence}_z g_{t,z}^\top, \quad (6)$$

with $g_{t,z} = \nabla_{\theta} \ell(\theta_t, z)$ and $W^{(T-1)} = \mathbf{0}$. We refer to this efficient implementation as SGD-influence throughout this paper.

B Derivation of AdamW-influence

This appendix gives the complete derivation of AdamW-influence. Since Section 3.1 states only an informal version of Proposition 1, we begin by establishing the full notation used in this appendix.

B.1 Setup and notation

AdamW updates. Consider a data point z^* that first participates in training at iteration t^* . The model is trained with AdamW: given the batch gradient $g_t = \nabla_{\theta} \ell(\theta_t, \mathcal{B}_t)$, the optimizer maintains first and second moment estimates

$$m_t = \beta_1 m_{t-1} + (1 - \beta_1) g_t, \quad v_t = \beta_2 v_{t-1} + (1 - \beta_2) g_t^2,$$

with bias-corrected versions $\hat{m}_t = m_t / (1 - \beta_1^{t+1})$ and $\hat{v}_t = v_t / (1 - \beta_2^{t+1})$. The parameter update is

$$\theta_{t+1} = (1 - \eta_t \lambda) \theta_t - \eta_t \frac{\hat{m}_t}{\sqrt{\hat{v}_t + \varepsilon}}.$$

We write $\theta_{t+1} = (1 - \eta_t \lambda) \theta_t - U_t$, where $U_t = \eta_t \hat{m}_t / (\sqrt{\hat{v}_t + \varepsilon})$, λ is the weight decay coefficient, and ε is the denominator smoothing term.

Gradient-level perturbation. As motivated in Section 3.1, AdamW’s update is nonlinear in the gradient through the second moment, so a parameter-level ϵ -injection (which is equivalent to gradient-level injection for SGD) does not correspond to removing z^* from the batch. We therefore inject the perturbation at the gradient level at step t^* :

$$g_{t^*}(\epsilon) = g_{t^*} - \epsilon g_{t^*,z^*}, \quad g_{t^*,z^*} := \nabla_{\theta} \ell(\theta_{t^*}, z^*),$$

so that $\epsilon = 0$ recovers the original trajectory and $\epsilon = 1$ removes z^* . Optimizer states before t^* are unaffected; all subsequent states are functions of ϵ . We use (\cdot) to denote the derivative with respect to ϵ evaluated at $\epsilon = 0$.

Auxiliary diagonal matrices. Throughout we use

$$D_t = \text{diag}\left(\frac{1}{\sqrt{\hat{v}_t + \varepsilon}}\right), \quad S_t = \text{diag}\left(\frac{\hat{m}_t}{2\sqrt{\hat{v}_t}(\sqrt{\hat{v}_t + \varepsilon})^2}\right),$$

which arise from differentiating U_t with respect to its inputs.

B.2 Initial derivatives at step t^*

Since all trajectories are identical before step t^* , the initial conditions are $\dot{\theta}_{t^*} = 0$, $\dot{m}_{t^*-1} = 0$, $\dot{v}_{t^*-1} = 0$. From the perturbed gradient, $\dot{g}_{t^*} = -g_{t^*,z^*}$.

The moment derivatives at the injection step are:

$$\dot{m}_{t^*} = \beta_1 \dot{m}_{t^*-1} + (1 - \beta_1) \dot{g}_{t^*} = -(1 - \beta_1) g_{t^*,z^*}, \quad (7)$$

$$\dot{v}_{t^*} = \beta_2 \dot{v}_{t^*-1} + 2(1 - \beta_2) \text{diag}(g_{t^*}) \dot{g}_{t^*} = -2(1 - \beta_2) \text{diag}(g_{t^*}) g_{t^*,z^*}. \quad (8)$$

The bias-corrected derivatives are $\dot{\hat{m}}_{t^*} = \dot{m}_{t^*} / (1 - \beta_1^{t^*+1})$ and $\dot{\hat{v}}_{t^*} = \dot{v}_{t^*} / (1 - \beta_2^{t^*+1})$.

Differentiating the update U_t coordinate-wise:

$$\dot{U}_{t^*,i} = \eta_{t^*} \left(\frac{\dot{m}_{t^*,i}}{\sqrt{\hat{v}_{t^*,i}} + \varepsilon} - \frac{\dot{m}_{t^*,i} \dot{v}_{t^*,i}}{2\sqrt{\hat{v}_{t^*,i}}(\sqrt{\hat{v}_{t^*,i}} + \varepsilon)^2} \right).$$

In vector form,

$$\dot{U}_{t^*} = \eta_{t^*} (D_{t^*} \dot{m}_{t^*} - S_{t^*} \dot{v}_{t^*}).$$

Substituting (7)–(8) and using $\dot{\theta}_{t^*+1} = -\dot{U}_{t^*}$:

$$\dot{\theta}_{t^*+1} = \eta_{t^*} \left(\frac{D_{t^*}}{1 - \beta_1^{t^*+1}} - \frac{2 S_{t^*} \text{diag}(g_{t^*})}{1 - \beta_2^{t^*+1}} \right) g_{t^*,z^*}. \quad (9)$$

The first term arises from the perturbation flowing through the first moment, while the second arises from the second moment. Assembling the three derivatives gives the initial state perturbation:

$$Z_{\text{push}}(z^*) = (\dot{\theta}_{t^*+1}^\top, \dot{m}_{t^*}^\top, \dot{v}_{t^*}^\top)^\top \in \mathbb{R}^{3p}. \quad (10)$$

B.3 Recurrence for $t \geq t^* + 1$

For all subsequent steps, the batch gradient has no direct ϵ -dependence (the only direct perturbation was at t^*), so $\dot{g}_t = \nabla_{\theta}^2 \ell(\theta_t, \mathcal{B}_t) \dot{\theta}_t = H_t \dot{\theta}_t$. The moment recurrences become

$$\begin{aligned} \dot{m}_t &= \beta_1 \dot{m}_{t-1} + (1 - \beta_1) H_t \dot{\theta}_t, \\ \dot{v}_t &= \beta_2 \dot{v}_{t-1} + 2(1 - \beta_2) \text{diag}(g_t) H_t \dot{\theta}_t, \end{aligned}$$

and the parameter recurrence is

$$\dot{\theta}_{t+1} = (1 - \eta_t \lambda) \dot{\theta}_t - \eta_t \left(\frac{D_t}{1 - \beta_1^{t+1}} \dot{m}_t - \frac{S_t}{1 - \beta_2^{t+1}} \dot{v}_t \right).$$

Augmented state and linear dynamical system. Because the gradient-level perturbation propagates jointly through the parameters and both moments, we lift the state to the augmented vector

$$Z_t = (\dot{\theta}_t^\top, \dot{m}_{t-1}^\top, \dot{v}_{t-1}^\top)^\top \in \mathbb{R}^{3p},$$

on which the perturbation evolves as a linear dynamical system $Z_{t+1} = A_t Z_t$. Collecting the recurrences above, the transition is

$$A_t = \begin{pmatrix} (1 - \eta_t \lambda) I - \frac{\eta_t(1 - \beta_1)}{1 - \beta_1^{t+1}} D_t H_t + \frac{2\eta_t(1 - \beta_2)}{1 - \beta_2^{t+1}} S_t \text{diag}(g_t) H_t & -\frac{\eta_t \beta_1}{1 - \beta_1^{t+1}} D_t & \frac{\eta_t \beta_2}{1 - \beta_2^{t+1}} S_t \\ 0 & \beta_1 I & 0 \\ 2(1 - \beta_2) \text{diag}(g_t) H_t & 0 & \beta_2 I \end{pmatrix}.$$

Decomposition into Hessian-free and Hessian-mediated parts. The transition admits a clean decomposition $A_t = M_t + R_t H_t P$, where $P = [I_p \ 0 \ 0] \in \mathbb{R}^{p \times 3p}$ extracts the parameter component, and

$$M_t = \begin{pmatrix} (1 - \eta_t \lambda) I & -\frac{\eta_t \beta_1}{1 - \beta_1^{t+1}} D_t & \frac{\eta_t \beta_2}{1 - \beta_2^{t+1}} S_t \\ 0 & \beta_1 I & 0 \\ 0 & 0 & \beta_2 I \end{pmatrix}, \quad (11a)$$

$$R_t = \begin{pmatrix} -\frac{\eta_t(1 - \beta_1)}{1 - \beta_1^{t+1}} D_t + \frac{2\eta_t(1 - \beta_2)}{1 - \beta_2^{t+1}} S_t \text{diag}(g_t) \\ (1 - \beta_1) I \\ 2(1 - \beta_2) \text{diag}(g_t) \end{pmatrix}. \quad (11b)$$

M_t collects the Hessian-free terms (momentum decay and weight decay), while R_t collects the Hessian-mediated coupling between optimizer states.

B.4 Backward recurrence for the summary matrix

Analogous to SGD-influence, we define a summary matrix $W^{(t)} \in \mathbb{R}^{p \times 3p}$ that encodes how a perturbation injected at step t propagates through all subsequent training steps to the final parameters: $W^{(t)} = P \Psi_t$, where $\Psi_t = \prod_{k=t}^{T-1} A_k$.

From $\Psi_t = A_t \Psi_{t+1}$ and the decomposition $A_t = M_t + R_t H_t P$, we obtain

$$W^{(t)} = P A_t \Psi_{t+1} = P(M_t + R_t H_t P) \Psi_{t+1}.$$

Using the block structure $P M_t = M_t^{(\theta)}$ where $M_t^{(\theta)}$ denotes the first block-row of M_t , together with $P \Psi_{t+1} = W^{(t+1)}$, the recurrence becomes

$$W^{(t)} = W^{(t+1)} M_t + (W^{(t+1)} R_t) H_t P,$$

where we used $P R_t = R_t^{(\theta)}$ and the fact that $W^{(t+1)}$ already absorbs P on the left. Substituting the GGN approximation $H_t \approx \frac{1}{|\mathcal{B}_t|} \sum_{z \in \mathcal{B}_t} g_{t,z} g_{t,z}^\top$ yields the per-sample form:

$$W^{(t)} = W^{(t+1)} M_t + \frac{1}{|\mathcal{B}_t|} \sum_{z \in \mathcal{B}_t} (W^{(t+1)} R_t g_{t,z}) g_{t,z}^\top P, \quad (12)$$

with terminal condition $W^{(T)} = [I \ 0 \ 0]$.

Per-sample influence. The estimated parameter change for sample z^* injected at step t^* is

$$\text{AdamW-influence}_{z^*} = W^{(t^*+1)} Z_{\text{push}}(z^*),$$

combining the initial perturbation (10) with the propagator (12). This recovers the formal version of Proposition 1: the recurrence (12) preserves the $\mathcal{O}(T)$ complexity of SGD-influence, with constant overhead reflecting the augmented state (cost analysis in Appendix C).

B.5 Sanity checks

SGD ($\beta_1 = \beta_2 = 0, \lambda = 0$). Setting $\beta_1 = \beta_2 = 0$ and removing the second moment (i.e., $S_t = 0, D_t = I$), the transition reduces to $\hat{\theta}_{t+1} = (I - \eta_t H_t) \hat{\theta}_t$, recovering the known SGD formula (Hara et al., 2019).

SGD with momentum ($\beta_1 > 0, \beta_2 = 0, \lambda = 0$). With $\beta_2 = 0, D_t = I, S_t = 0$, and neglecting bias correction, the system becomes:

$$\begin{pmatrix} \hat{\theta}_{t+1} \\ \dot{m}_t \end{pmatrix} = \begin{pmatrix} I - \eta_t(1 - \beta_1)H_t & -\eta_t \beta_1 I \\ (1 - \beta_1)H_t & \beta_1 I \end{pmatrix} \begin{pmatrix} \hat{\theta}_t \\ \dot{m}_{t-1} \end{pmatrix},$$

recovering the known SGD-momentum formula (Zhang et al., 2025).

B.6 AdamW-influence: algorithm

Algorithm 1 summarizes the backward recurrent computation of AdamW-influence.

C Efficient computation and storage of AdamW-influence

C.1 Random masking and ensembles

The per-sample gradient and momentums cached by AdamW-influence live in \mathbb{R}^p , where p is the number of model parameters. Storing and manipulating p -dimensional embedding per training sample is prohibitive at modern scale, so dimensionality reduction is essential.

SGD-influence (Wang et al., 2025b) admits an efficient random-projection implementation because its backward recurrence is linear in the per-sample gradients, so the Johnson–Lindenstrauss lemma preserves the relevant inner products under a random projection. AdamW-influence breaks this property: the matrices D_t and S_t in Eqs. 11 apply a coordinate-wise nonlinearity to \hat{v}_t , which a random projection scrambles.

Random masking. We sample once a fixed binary mask $\mathbf{m} \in \{0, 1\}^p$, and restrict the entire AdamW-influence computation to the index set $\mathcal{S} = \{i : \mathbf{m}_i = 1\}$. All per-sample gradients $g_{t,z}$, batch gradients g_t , and optimizer states are subselected to \mathcal{S} so Algorithm 1 remains the same with p replaced by $|\mathcal{S}|$. The mask is shared across all training steps and samples within a single run.

Algorithm 1 Backward Recurrent algorithm of AdamW-influence

Require: Training batches $\{\mathcal{B}_t\}_{t=0}^{T-1}$ with per-sample gradients $\{g_{t,z}\}_{z \in \mathcal{B}_t}$, optimizer states $\{m_t, v_t\}_{t=0}^{T-1}$, learning rates $\{\eta_t\}$, exponential decay rates β_1, β_2 , weight decay coefficient λ , and denominator smoothing term ε .

Ensure: AdamW-influence embeddings $\{\text{AdamW-influence}_z\}_{z \in \mathcal{D}}$

- 1: $W \leftarrow [I \ 0 \ 0] \in \mathbb{R}^{p \times 3p}$ ▷ Initialize summary matrix
- 2: **for** $t = T - 1$ **down to** 0 **do**
- 3: Compute $D_t = \text{diag}(1/(\sqrt{\hat{v}_t} + \varepsilon))$, $S_t = \text{diag}(\hat{m}_t/(2\sqrt{\hat{v}_t}(\sqrt{\hat{v}_t} + \varepsilon)^2))$
- 4: Construct M_t from Eq. (11a) and R_t from Eq. (11b)
- 5: **for** $z \in \mathcal{B}_t$ **do** ▷ Use $g_{t,z}/|\mathcal{B}_t|$ for mean reduction
- 6: $\hat{m}_t \leftarrow -(1 - \beta_1) g_{t,z}$
- 7: $\hat{v}_t \leftarrow -2(1 - \beta_2) g_t \odot g_{t,z}$
- 8: $\dot{m}_t \leftarrow \hat{m}_t/(1 - \beta_1^{t+1})$, $\dot{v}_t \leftarrow \hat{v}_t/(1 - \beta_2^{t+1})$
- 9: $\dot{\theta}_{t+1} \leftarrow -\eta_t(D_t \dot{m}_t - S_t \dot{v}_t)$
- 10: $Z_{\text{push}}(z) \leftarrow (\dot{\theta}_{t+1}^\top, \dot{m}_t^\top, \dot{v}_t^\top)^\top$
- 11: $\text{AdamW-influence}_z \leftarrow W Z_{\text{push}}(z)$
- 12: **end for**
- 13: $\Delta W \leftarrow 0$
- 14: **for** $z \in \mathcal{B}_t$ **do**
- 15: $v \leftarrow W R_t g_{t,z}$, $u^\top \leftarrow (g_{t,z}^\top, 0, 0)$
- 16: $\Delta W \leftarrow \Delta W + v u^\top$
- 17: **end for**
- 18: $W \leftarrow W M_t + \frac{1}{|\mathcal{B}_t|} \Delta W$
- 19: **end for**
- 20: **return** $\{\text{AdamW-influence}_z\}_{z \in \mathcal{D}}$

Ensembles for masking. At the LLM scale, memory constraints push $|\mathcal{S}|/p$ to small values, where a single mask produces significant variance and information loss. We mitigate this with an ensemble of M independent masks, run AdamW-influence once per mask to obtain scores, and aggregate by simple average. Per-setting choices of M are reported in Appendix D.

C.2 Computational efficiency

We compare the cost of AdamW-influence against SGD-influence along three axes: per-sample embedding storage, working memory during the backward recurrence, and per-step compute. Throughout this section, p denotes the number of model parameters, T the number of training steps, b the batch size, and $|\mathcal{S}|$ the number of coordinates retained after random masking ($|\mathcal{S}| = p$ if masking is disabled). For ease of exposition, we first describe costs in terms of p and then note that masking replaces p with $|\mathcal{S}|$ throughout, providing the same multiplicative cost reduction as random projection in SGD-influence.

Working memory and storage. The summary matrix $W^{(t)} \in \mathbb{R}^{p \times 3p}$ is $3 \times$ larger than the $\mathbb{R}^{p \times p}$ matrix in SGD-influence, reflecting the extended state $(\dot{\theta}, \dot{m}, \dot{v})$ that AdamW-influence must propagate. Per-step trajectory caching incurs a similar additive overhead: AdamW-influence stores \hat{m}_t, \hat{v}_t alongside the per-sample gradients $\{g_{t,z}\}_{z \in \mathcal{B}_t}$ and batch gradient g_t , adding $2p$ per step on top of the $bp + p$ already required by SGD-influence. When b is not too small, this overhead is dominated by the bp per-sample gradient term and is $\mathcal{O}(1/b)$ relative to it.

Per-step compute. The dominant cost in the backward recurrence is the update of $W^{(t)}$ in Eq. 12. The term $W^{(t+1)} M_t$ exploits the block structure of M_t (each block is either diagonal or a scalar multiple of identity), so it costs $\mathcal{O}(p^2)$. The per-sample term $W^{(t+1)} R_t g_{t,z}$ similarly leverages the block structure of R_t , costing $\mathcal{O}(p^2)$ per sample, and the rank-one update to $W^{(t)}$ costs $\mathcal{O}(3p^2)$ per sample due to the wider second dimension. The total per-step cost is $\mathcal{O}(3bp^2)$, compared to $\mathcal{O}(bp^2)$ for SGD-influence, a $3 \times$ overhead arising directly from the wider summary matrix.

Effect of random masking. With masking, every p above is replaced by $|\mathcal{S}|$. The $3 \times$ ratios between AdamW-influence and SGD-influence are preserved. Random masking thus delivers the same form of cost reduction that random projection provides in SGD-influence—turning otherwise infeasible quadratic costs in p into tractable quadratic costs in $|\mathcal{S}|$ —without breaking the coordinate-wise structure required by AdamW (Section C.1). In summary, AdamW-influence

incurs a $3\times$ overhead in working memory and per-step compute relative to SGD-influence, while keeping the per-sample embedding size identical.

Table 2: Cost comparison between SGD-influence and AdamW-influence. The first four rows describe the per-component costs without masking; the last two row gives the total cost when random masking without/with $|\mathcal{S}|$ retained coordinates is applied. The $3\times$ ratios are preserved under masking.

	SGD-influence	AdamW-influence	Ratio (Adam / SGD)
Per-sample embedding (storage)	p	p	$1\times$
Summary matrix W (memory)	p^2	$3p^2$	$3\times$
Trajectory cache (per step)	$bp + p$	$bp + 3p$	$\approx 1\times$
Backward recurrence (per step)	$\mathcal{O}(bp^2)$	$\mathcal{O}(3bp^2)$	$3\times$
Total cost	$\mathcal{O}(Tbp^2)$	$\mathcal{O}(3Tbp^2)$	$3\times$
Total cost (with masking \mathcal{S})	$\mathcal{O}(Tb \mathcal{S} ^2)$	$\mathcal{O}(3Tb \mathcal{S} ^2)$	$3\times$

D Experiment details

D.1 Experimental settings for fidelity evaluation

In section 3.2, we consider four experiment settings to evaluate the attribution fidelity of AdamW-influence. We also consider additional settings presented in Appendix E.

- **MNIST+MLP.** We train a three-layer multilayer perceptron (MLP) with hidden layer sizes of 16, consisting of two fully connected layers ($28 \times 28 \rightarrow 16 \rightarrow 16$) with ReLU activations, followed by a final linear layer mapping to 10 output classes on the MNIST dataset (LeCun et al., 2002). We train on 10% of MNIST for 1 epoch. We set the batch size to 64 and perform the experiment on 5 learning rates (10^{-2} , 10^{-3} , 10^{-4} , 10^{-5} and 10^{-6}). TSLOO ground truth is computed for 200 randomly selected training samples. The Spearman correlation is computed across these 200 samples and averaged over 500 validation points. We use AdamW, we set $\beta_1 = 0.9$ and $\beta_2 = 0.95$.
- **MNIST+CNN.** We train a convolutional neural network (CNN) with two convolutional layers (Conv2d(1, 32, 3, padding=1) and Conv2d(32, 64, 3, padding=1), each followed by ReLU and 2×2 max pooling) and a final fully connected layer of size $64 \times 7 \times 7 \rightarrow 10$ on the MNIST dataset (LeCun et al., 2002). We train on 10% of MNIST for one epoch. We set the batch size to 64 and perform the experiment on 5 learning rates (10^{-2} , 10^{-3} , 10^{-4} , 10^{-5} , 10^{-6}). We use a random masking ratio of 0.75 with a single masking ensemble. TSLOO ground truth is computed for 200 randomly selected training samples. The Spearman correlation is computed across these 200 samples and averaged over 500 validation points. We use AdamW, we set $\beta_1 = 0.9$ and $\beta_2 = 0.95$.
- **WikiText-2+GPT-2.** We continually pretrain a GPT-2 language model Radford et al. (2019) on the WikiText-2 dataset Merity et al. (2016) by splitting the corpus into non-overlapping token blocks. GPT-2 is licensed under MIT license and WikiText-2 is licensed under CC BY-SA 3.0. We experiment with multiple training configurations, changing the number of training samples and block sizes, specifically: 512 and 1024 training samples with block sizes of 128 and 256. All models are trained for three epochs. We use the AdamW optimizer with three learning rates (1×10^{-4} , 5×10^{-5} , and 1×10^{-5}) and a linear learning rate scheduler with warmup. We set the batch size to 32 and use a random masking ensemble of size 10 with projection dimension 512. TSLOO ground truth is computed for 50 randomly selected training samples. The Spearman correlation is computed across these 50 samples and averaged over 256 validation points.
- **Alpaca + Llama 3.2-1B.** We fine-tune a LLaMA-3.2-1B language model (Grattafiori et al., 2024) on the Alpaca instruction-tuning dataset (Taori et al., 2023), using the first 512 training examples with a maximum sequence length of 512 tokens. We train for 1 epoch and evaluate attribution fidelity on 100 test samples from the SAMSum summarization task (Gliwa et al., 2019). We use the AdamW optimizer and sweep learning rates spanning 5×10^{-7} , 2×10^{-6} , and 6×10^{-6} ($\beta_1 = 0.9$, $\beta_2 = 0.999$, max gradient norm 1.0) and a linear learning-rate scheduler with 100 warmup steps. We evaluate both AdamW-influence and SGD-influence. We set the batch size to 8 and use a random-masking ensemble of size 10 with projection dimension 256. TSLOO ground truth is computed for 50 randomly selected training samples. The Spearman correlation is computed across these 50 samples; attribution scores are then compared against TSLOO effects on 256 SAMSum (Gliwa et al., 2019) test samples.

D.2 Experimental settings for dissecting algorithm-level error

In Section 4, we conduct three analyses on the algorithm-level error of AdamW-influence: (i) decomposing the absolute SGD-influence error into config-level, algorithm-level, and residual components (Section 4.1, Figure 2); (ii) sweeping learning rates to identify the two governing factors of the algorithm-level error (Section 4.2, Figure 3); and (iii) validating the closed-form error proxy against ground-truth update-estimation error norms (Section 4.3, Figure 4). All experiments are conducted on the MNIST+MLP and MNIST+CNN settings; model architecture, dataset preparation, batch size, optimizer hyperparameters ($\beta_1 = 0.9$, $\beta_2 = 0.95$), random masking configuration, and the number of LOO training samples (200) and TSLOO validation samples (500) follow Appendix D.1. Below we describe only the analysis-specific details.

- **Error decomposition (Section 4.1, Figure 2).** We use the MNIST+MLP setting and sweep three learning rates (10^{-3} , 10^{-4} , 10^{-5}). For each sample z^* , we compute its absolute SGD-influence error against the TSLOO ground truth and decompose it into the three additive components in Equation (4): the optimizer-mismatch share (green), the update-estimation error remaining after optimizer alignment (blue), and the higher-order residual (grey). Errors from samples whose injection step t^* falls within the same 5-step window are aggregated into a single bin, yielding the binned curves shown in Figure 2.
- **Sweep of governing factors (Section 4.2, Figure 3).** We use the MNIST+MLP and MNIST+CNN settings and sweep three learning rates (10^{-3} , 10^{-4} , 10^{-5}). For each (z^*, t^*) pair, we compute two metrics: (i) the parameter-space error norm $\|\Delta\theta_{z^*} - \text{AdamW-influence}_{z^*}\|_2$, where $\Delta\theta_{z^*}$ is obtained by trajectory-specific LOO retraining; and (ii) the intra-step Spearman correlation between AdamW-influence scores and ground-truth TSLOO scores computed over all samples sharing the same injection step t^* . The intra-step correlation curves in Figure 3(b, d) are smoothed by a rolling mean over a window of 5 consecutive training steps to reduce step-to-step noise; the error-norm curves in Figure 3(a, c) are reported without smoothing.
- **Error proxy validation (Section 4.3, Figure 4).** We use the MNIST+MLP and MNIST+CNN settings, each at two learning rates (10^{-3} and 10^{-4}). For every training sample (4992 in total per setting), we compute the closed-form error proxy from Equation (4) along the original training trajectory, alongside the ground-truth update-estimation error norm $\|\Delta\theta_{z^*} - \text{AdamW-influence}_{z^*}\|_2$ obtained via trajectory-specific LOO retraining. Each point in Figure 4 corresponds to one training sample; the reported Spearman ρ , slope, and R^2 are computed across all 4992 samples per panel.

D.3 Experimental settings for data selection

In Section 5, we evaluate the unified K -step look-ahead framework on four settings: MNIST+MLP, MNIST+CNN, Tulu3+Llama 3.2-1B, and Alpaca+Llama 3.2-1B. Across all three settings, we compare three methods: *offline AdamW-influence*, *online SGD-influence*, and *online AdamW-influence*. Offline AdamW-influence does not involve K , since it scores candidates against a completed reference trajectory and retrains from scratch on the selected subset. For online methods, the look-ahead horizon K is swept and the best K per setting (selected by validation performance) is reported in Figure 5: $K = 10$ for MNIST+MLP, $K = 2$ for Tulu3+Llama 3.2-1B, and $K = 2$ for Alpaca+Llama 3.2-1B. Section 5.2 additionally sweeps $K \in \{2, 5, 10, 25\}$ across three learning rates on MNIST+MLP (Figure 6). Below we describe the per-setting details.

- **MNIST+MLP.** Model architecture and dataset preparation follow Appendix D.1. We train for 20 epochs (rather than 1 epoch as in fidelity evaluation) to allow the model to converge under the reduced effective batch size induced by selection. At each training step, the candidate batch size is $N = 64$ and the final batch size after selection is $B = 32$, corresponding to a selected ratio of 0.5. For Figure 5, we use learning rate 10^{-3} and $K = 10$. For the K -sweep in Figure 6, we sweep $K \in \{2, 5, 10, 25\}$ across three learning rates $\{10^{-2}, 10^{-3}, 10^{-4}\}$. Validation and test error rates are reported at the best validation epoch.
- **MNIST+CNN.** Model architecture and dataset preparation follow Appendix D.1. We train for 20 epochs (rather than 1 epoch as in fidelity evaluation) to allow the model to converge under the reduced effective batch size induced by selection. At each training step, the candidate batch size is $N = 64$ and the final batch size after selection is $B = 32$, corresponding to a selected ratio of 0.5. For Figure 5, we use learning rate 10^{-3} and $K = 5$. For the K -sweep in Figure 6, we sweep $K \in \{2, 5, 10\}$ across three learning rates $\{10^{-2}, 10^{-3}, 10^{-4}\}$. Validation and test error rates are reported at the best validation epoch.
- **Alpaca+Llama 3.2-1B.** Model, optimizer hyperparameters ($\beta_1 = 0.9$, $\beta_2 = 0.999$, max gradient norm 1.0), maximum sequence length (512 tokens), training batch size (8), random-masking ensemble of size 10 with projection dimension 256, and linear learning-rate scheduler with 100 warmup steps follow Appendix D.1. We deviate from the fidelity setup as follows: (i) we use 40% of the Alpaca dataset for training (rather than the

first 512 examples); (ii) we use a learning rate of 2×10^{-6} ; (iii) full fine-tuning is used (no LoRA); (iv) the candidate batch size is $N = 8$ and the selected ratio is 0.8, so $B = 6$ samples are retained per step; and (v) validation uses 16 randomly sampled SAMSum examples for online method selection, and final evaluation is reported on the full SAMSum test set. Validation and test perplexity are reported at the final training step.

- **Tulu3+Llama 3.2-1B.** The training setup mirrors the Alpaca+Llama 3.2-1B configuration above, with the following differences: (i) we use 1% of the Tulu3 dataset for training; (ii) the learning rate is 4×10^{-5} for full fine-tuning (used in Figure 5) and 3×10^{-3} for LoRA fine-tuning (used only in Tables 5 and 6 of Appendix E.2); (iii) the candidate batch size is $N = 8$ and the selected ratio is 0.5, so $B = 4$ samples are retained per step; and (iv) validation uses 16 randomly sampled tydiqa (Clark et al., 2020) examples for online method selection, and final evaluation is reported on the full tydiqa test set. Validation and test perplexity are reported at the final training step.
- **Additional baseline in Tables 5 and 6.** The Tulu3+Llama 3.2-1B results in Appendix E.2 additionally include TracIn (Pruthi et al., 2020) as an offline baseline, and sweep both fine-tuning regime (full vs. LoRA) and selected ratio (0.5 vs. 0.8). All other training and evaluation details follow the Tulu3+Llama 3.2-1B configuration above.

D.4 Compute Resources

The experiment is carried out on A100 GPUs. The total GPU hour required for the experiments is around 400 hours.

E Additional Experiment Results

E.1 Fidelity additional results

Tables 3 and 4 together demonstrate that attribution fidelity hinges on aligning the attribution formula with the actual training optimizer. Table 3 extends Table 1 to additional data sizes and learning rates: when training with AdamW, AdamW-influence consistently outperforms SGD-influence across all four settings, with relative improvements ranging from 10% to over 300%. The improvement is especially large at higher learning rates, where the SGD update fails most dramatically as a proxy for the AdamW update. We also reported the error bar under 10 independent runs for MNIST experiments and 5 independent runs for GPT-2 / Llama 3.2 experiments.

Table 4 reports the symmetric sanity check: when the model is instead trained with SGD, SGD-influence dominates AdamW-influence by a similarly wide margin. This is the expected behavior. Under SGD training, the cached optimizer states g_t, m_t, v_t that AdamW-influence relies on are computed along an SGD trajectory rather than an AdamW one, so AdamW-influence is unrolling an optimizer that the model never actually used. The result confirms that the gains in Table 3 come from *matching* the attribution formula to the training optimizer, not from any intrinsic superiority of AdamW-influence over SGD-influence: each method attributes faithfully only when its assumed optimizer matches the one used in training.

E.2 Data selection additional results

Tables 5 and 6 extend the Tulu3 results in Section 5.2 along two practical axes: the fine-tuning regime (full fine-tuning vs. LoRA) and the selected data ratio (0.5 vs. 0.8). Online AdamW-influence achieves the lowest perplexity across all eight configurations on both validation and test splits.

F Derivation of Proposition 2

This appendix derives Proposition 2 (the closed-form error proxy in Section 4.3). All notation follows Appendix B.1: D_t and S_t are the diagonal matrices defined there, and $(\dot{\cdot})$ denotes derivatives with respect to the gradient-level perturbation scalar ϵ at $\epsilon = 0$. We treat $\lambda = 0$; the extension to $\lambda > 0$ replaces each $(I - A_k^{\text{eff}})$ below with $((1 - \eta_k \lambda)I - A_k^{\text{eff}})$ and leaves $r_t(0)$ unchanged.

F.1 Error recursion

Recall the AdamW update $\theta_{t+1}(\epsilon) = \theta_t(\epsilon) - U_t(\epsilon)$ with $U_t = \eta_t \hat{m}_t / (\sqrt{\hat{v}_t} + \epsilon)$, and its linearization $\dot{\theta}_{t+1} = \dot{\theta}_t - \dot{U}_t$. Define

$$e_t := [\theta_t(1) - \theta_t(0)] - \dot{\theta}_t, \quad r_t := [U_t(1) - U_t(0)] - \dot{U}_t.$$

Table 3: Full fidelity comparison (Spearman ρ against TSLOO ground truth) between AdamW-influence and SGD-influence when training with **AdamW**, across varying epochs, data sizes, and learning rates. Best result per row in **bold**. Δ is the relative improvement of AdamW-influence over SGD-influence.

Setting	Epochs	Data Size	LR	AdamW-influence	SGD-influence	Δ
MNIST+MLP	1	4992	1e-2	0.043±0.003	0.023±0.004	+87%
			1e-3	0.205±0.011	0.075±0.009	+173%
			1e-4	0.294±0.014	0.242±0.016	+21%
			1e-5	0.786±0.013	0.715±0.012	+10%
			1e-6	0.948±0.006	0.833±0.011	+14%
MNIST+CNN	1	4992	1e-2	0.048±0.008	0.027±0.011	+74%
			1e-3	0.090±0.008	0.015±0.009	+500%
			1e-4	0.511±0.017	0.122±0.015	+319%
			1e-5	0.791±0.007	0.526±0.007	+50%
			1e-6	0.767±0.013	0.523±0.009	+47%
WikiText+GPT-2	3	65K (block size= 128)	1e-4	0.734±0.003	0.372±0.006	+97%
			5e-5	0.825±0.002	0.432±0.009	+91%
			1e-5	0.842±0.006	0.480±0.015	+75%
		131K (block size= 256)	1e-4	0.672±0.009	0.321±0.011	+109%
			5e-5	0.787±0.003	0.383±0.011	+105%
			1e-5	0.810±0.009	0.420±0.011	+93%
262K (block size= 256)	1e-4	0.327±0.013	0.158±0.013	+107%		
	5e-5	0.471±0.012	0.223±0.009	+111%		
	1e-5	0.785±0.008	0.393±0.007	+100%		
Alpaca+Llama 3.2	1	512	6e-6	0.276±0.047	0.156±0.019	+77%
			2e-6	0.342±0.036	0.197±0.007	+74%
			5e-7	0.665±0.013	0.330±0.017	+102%

Table 4: Fidelity comparison (Spearman ρ against TSLOO ground truth) between AdamW-influence and SGD-influence when training with **SGD**, across varying epochs, data sizes, and learning rates. Best result per row in **bold**.

Setting	Epochs	Data Size	LR	AdamW-influence	SGD-influence
MNIST+MLP	1	4992	1e-2	0.015±0.004	0.349±0.016
			1e-3	0.047±0.005	0.707±0.023
			1e-4	0.447±0.017	0.939±0.012
			1e-5	0.746±0.015	0.968±0.001
			1e-6	0.833±0.010	0.969±0.001
MNIST+CNN	1	4992	1e-2	0.042±0.004	0.389±0.015
			1e-3	0.036±0.006	0.808±0.009
			1e-4	0.061±0.006	0.599±0.011
			1e-5	0.461±0.009	0.613±0.015
			1e-6	0.480±0.010	0.616±0.016

Subtracting the linearized recursion from the true one gives $e_{t+1} = e_t - r_t$ with $e_{t^*} = 0$.

Although $U_t(1)$ is evaluated on the ground-truth retrained trajectory $\theta_t(1)$, expressing $\theta_t(1) = \theta_t(0) + \dot{\theta}_t + e_t$ and Taylor-expanding U_t around $\theta_t(0)$ introduces an e_t -dependence:

$$r_t(e_t) \approx r_t(0) + A_t^{\text{eff}} e_t, \quad A_t^{\text{eff}} := \left. \frac{\partial U_t}{\partial \theta_t} \right|_{\theta_t(0)} = \eta_t \frac{1 - \beta_1}{1 - \beta_1^{t+1}} D_t H_t - 2\eta_t \frac{1 - \beta_2}{1 - \beta_2^{t+1}} S_t \text{diag}(g_t) H_t,$$

Table 5: Evaluation perplexity on Tulu3 (tydiqa) with Llama-3.2-1B. Lower is better; **bold** indicates the best result per column.

Method \ Selected Ratio	Full		LoRA	
	0.5	0.8	0.5	0.8
TracIN (offline)	2.152±0.063	2.175±0.081	1.955±0.027	1.910±0.065
SGD-influence (online)	2.029±0.034	2.055±0.077	1.810±0.026	1.872±0.016
AdamW-influence (offline)	1.957±0.021	1.939±0.017	1.868±0.028	1.872±0.061
AdamW-influence (online)	1.886±0.045	1.933±0.018	1.764±0.021	1.859±0.012

Table 6: Validation perplexity on Tulu3 (tydiqa) with Llama-3.2-1B. Lower is better; **bold** indicates the best result per column.

Method \ Selected Ratio	Full		LoRA	
	0.5	0.8	0.5	0.8
TracIN (offline)	2.066±0.087	2.154±0.140	1.811±0.035	1.872±0.069
SGD-influence (online)	1.849±0.057	1.857±0.022	1.729±0.017	1.730±0.054
AdamW-influence (offline)	1.836±0.042	1.874±0.018	1.803±0.042	1.836±0.062
AdamW-influence (online)	1.742±0.025	1.776±0.041	1.707±0.042	1.723±0.063

where $r_t(0)$ is the residual evaluated on the unperturbed trajectory and A_t^{eff} follows from differentiating U_t through the moment recurrences. Substituting yields $e_{t+1} = (I - A_t^{\text{eff}})e_t - r_t(0)$, which unrolls to

$$e_T = - \sum_{t=t^*}^{T-1} \left[\prod_{k=t+1}^{T-1} (I - A_k^{\text{eff}}) \right] r_t(0). \quad (13)$$

When $\|A_t^{\text{eff}}\| \ll 1$, the propagation factor $\prod_k (I - A_k^{\text{eff}}) \approx I$ and the proxy simplifies to $e_T \approx - \sum_t r_t(0)$, which we use to compute Figure 4.

F.2 Magnitude of $r_t(0)$

Writing $U_{t,i} = \eta_t f_{t,i}$ with $f_{t,i}(\epsilon) = \hat{m}_{t,i}(\epsilon) / (\sqrt{\hat{v}_{t,i}(\epsilon)} + \epsilon)$, we have $r_{t,i}(0) = \frac{1}{2} \eta_t \ddot{f}_{t,i}|_{\epsilon=0}$. Let $h_i := \sqrt{\hat{v}_{t,i}} + \epsilon$. Direct differentiation gives

$$\ddot{f}_{t,i} = \frac{\ddot{m}_{t,i}}{h_i} - \frac{\dot{m}_{t,i} \dot{h}_i}{h_i^2} - \frac{2 \dot{m}_{t,i} \dot{h}_i}{h_i^2} + \frac{2 \dot{m}_{t,i} \dot{h}_i^2}{h_i^3}, \quad (14)$$

with $\dot{h}_i = \dot{\hat{v}}_{t,i} / (2\sqrt{\hat{v}_{t,i}})$ and $\ddot{h}_i = \ddot{\hat{v}}_{t,i} / (2\sqrt{\hat{v}_{t,i}}) - \dot{\hat{v}}_{t,i}^2 / (4\hat{v}_{t,i}^{3/2})$.

At $t > t^*$, the moment derivatives admit the leading-order expressions (suppressing bias-correction prefactors):

$$\dot{m}_{t,i} \sim [H_t \dot{\theta}_t]_i, \quad \ddot{m}_{t,i} \sim \sum_{j,k} [\nabla^3 \ell_t]_{ijk} \dot{\theta}_{t,j} \dot{\theta}_{t,k} \sim \|\dot{\theta}_t\|^2, \quad \dot{h}_i \sim \frac{g_{t,i} \dot{g}_{t,i}}{\sqrt{\hat{v}_{t,i}}}, \quad \ddot{h}_i \sim \frac{\dot{g}_{t,i}^2}{\sqrt{\hat{v}_{t,i}}}.$$

Using $h_i \approx \sqrt{\hat{v}_{t,i}}$ and the Adam normalization $\dot{m}_{t,i} / \sqrt{\hat{v}_{t,i}} = \mathcal{O}(1)$, the four terms in (14) scale as $\|\dot{\theta}_t\|^2 / \sqrt{\hat{v}_{t,i}}$, $[H_t \dot{\theta}_t]_i^2 / \hat{v}_{t,i}$, and (for terms 3 and 4) $[H_t \dot{\theta}_t]_i^2 / \hat{v}_{t,i}$ further suppressed by $|g_{t,i}| / \sqrt{\hat{v}_{t,i}} \leq 1$ (the batch-mean gradient is bounded above by the per-coordinate RMS accumulated by Adam). Terms 1 and 2 dominate, giving

$$|r_{t,i}(0)| = \frac{1}{2} \eta_t |\ddot{f}_{t,i}| \sim \eta_t \left(\frac{\|\dot{\theta}_t\|^2}{\sqrt{\hat{v}_{t,i}}} + \frac{[H_t \dot{\theta}_t]_i^2}{\hat{v}_{t,i}} \right), \quad (15)$$

which recovers the residual bound stated in Proposition 2. The first term originates from the loss nonlinearity ($\nabla^3 \ell$) entering $\ddot{m}_{t,i}$ and is present even for non-adaptive optimizers; the second originates from the quadratic dependence of \hat{v}_t on gradient perturbations and is specific to Adam-family optimizers. Both belong to a single second-order remainder of $f_{t,i}$ and are not independent error sources.

G Pseudo-code of the unified K -step selection loop

Algorithm 2 summarizes the unified K -step look-ahead data selection loop introduced in Section 5.1.

Algorithm 2 K -step look-ahead data selection

Require: Candidate batch size N ; training batch size B ; look-ahead horizon K ; validation set V

```

1: Initialize model parameters
2: for each training step  $t$  do
3:   Sample a candidate batch of  $N$  examples from the stream
4:   for each candidate  $z$  in the candidate batch do
5:     Score  $z$  by how much including  $z$  now would reduce validation loss on  $V$ , evaluated  $K$  steps later
6:   end for
7:   Keep the top- $B$  candidates as the training batch
8:   Update model parameters on the selected training batch
9: end for
10: return trained model

```

Two boundary cases are worth highlighting. $K = 0$ recovers the per-step scoring rule used by GREATS Wang et al. (2024) (without its greedy selection iteration). The limit of K equal to the remaining training steps is the full-trajectory horizon; it is intractable in the online loop and is instead approximated by offline selection on a completed reference trajectory.